J Biol Phys (2009) 35:279–295
DOI 10.1007/s10867-009-9167-7

ORIGINAL PAPER

Pulsed-laser creation and characterization of giant plasma membrane vesicles from cells

Christopher V. Kelly · Mary-Margaret T. Kober · Päivö Kinnunen · David A. Reis · Bradford G. Orr · Mark M. Banaszak Holl

Received: 8 January 2009 / Accepted: 21 May 2009 /
Published online: 20 June 2009

Abstract Femtosecond-pulsed laser irradiation was found to initiate giant plasma membrane vesicle (GPMV) formation on individual cells. Laser-induced GPMV formation resulted from intracellular cavitation and did not require the addition of chemical stressors to the cellular environment. The viscosity, structure, and contents of laser-induced GPMVs

Electronic supplementary material The online version of this article (doi: 10.1007/s10867-009-9167-7) contains supplementary material, which is available to authorized users.

Mary-Margaret T. Kober and Päivö Kinnunen gave equal contribution to this manuscript.

C. V. Kelly · D. A. Reis · B. G. Orr · M. M. Banaszak Holl
Applied Physics Program, University of Michigan, Ann Arbor, MI, USA

C. V. Kelly · M. M. Banaszak Holl
Biophysics, University of Michigan, Ann Arbor, MI, USA

C. V. Kelly · M. M. Banaszak Holl
Graham Environmental Sustainability Institute, University of Michigan, Ann Arbor, MI, USA

C. V. Kelly · M.-M. T. Kober · P. Kinnunen · B. G. Orr · M. M. Banaszak Holl
Michigan Nanotechnology Institute for Medicine and Biological Sciences, University of Michigan, Ann Arbor, MI, USA

M.-M. T. Kober · M. M. Banaszak Holl
Department of Chemistry, University of Michigan, Ann Arbor, MI, USA

P. Kinnunen · D. A. Reis · B. G. Orr
Department of Physics, University of Michigan, Ann Arbor, MI, USA

B. G. Orr (✉)
450 Church Street, Ann Arbor, MI 48109, USA
e-mail: orr@umich.edu

M. M. Banaszak Holl (✉)
930 North University Avenue, Ann Arbor, MI 48109, USA
e-mail: mbanasza@umich.edu

were measured with fluorescence microscopy and single-particle tracking. These GPMVs exhibit the following properties: (1) GPMVs grow fastest immediately after laser irradiation; (2) GPMVs contain barriers to free diffusion of incorporated fluorescent beads; (3) materials from both the cytoplasm and surrounding media flow into the growing GPMVs; (4) the GPMVs are surrounded by phospholipids, including phosphatidylserine; (5) F-actin is incorporated into the vesicles; and (6) caspase activity is not essential for GPMV formation. The effective viscosity of 65 nm polystyrene nanoparticles within GPMVs ranged from 32 to 434 cP. The nanoparticle diffusion was commonly affected by relatively large, macromolecular structures within the bleb.

Keywords Giant plasma membrane vesicle (GPMV) · Single-particle tracking · Membrane permeability · Micro-bubble · Viscosity · Bleb · Femtosecond laser pulse

1 Introduction

Giant plasma membrane vesicles (GPMVs), or blebs, are fluid-filled membrane-bound protrusions from the extracellular surface of living cells. GPMVs result when the cortical actin can no longer contain the intracellular pressure, resulting in a separation of the plasma membrane from the cytoskeleton [1–8]. GPMVs are naturally created during cell death, division, locomotion, signal transduction, or apoptosis. GPMV formation is generally controlled by the cell through regulation of the cortical actin and plasma membrane by complex cellular systems [9–11]. These natural GPMVs are reversible and triggered by a protein-mediated, temporary, asymmetric loss of cortical actin integrity and are later retracted back into the cell [4, 11–15]. In contrast, irreversible GPMVs may result from a burn, blunt trauma, hypoxia, inflammation, poison, or infection when a sudden stress induces cortical actin and plasma membrane separation [2, 5–7, 16–21]. These irreversible GPMVs are an uncontrolled cellular response, are associated with necrosis, and are occasionally called cell blisters [18, 19, 22]. Reversible blebbing has been well studied, but little is known of the underlying biophysics of irreversible GPMVs. These irreversible, stress-induced GPMVs are the focus of this study.

Irreversible GPMVs are interesting in the context of understanding physiological processes that result from necrosis, such as minimizing inflammation and scarring. Irreversible GPMVs have also been used as a model system for the plasma membrane. With GPMVs harvested from cell cultures, fundamental membrane properties can be more easily examined. GPMVs previously have been used to better understand local variations in membrane phase, tension, and curvature [16, 23, 24] in addition to the structure [25], diffusion [26], and distribution of proteins on the plasma membrane [27, 28].

All studies that previously characterized irreversible blebs used bulk chemical or physical treatments and affected all the cells within the culture. The ability to trigger GPMV formation with pulsed lasers is distinct from previously reported bulk methods because it allows controlled studies on a single cell in close proximity to unaffected control cells. Additionally, laser irradiation allows for more specific control of the applied stress parameters than bulk methods, including control of laser pulse duration, rate, intensity, and focal spot location.

The intense electromagnetic fields of pulsed-laser systems provide advantages by inducing multi-photon processes such as sub-diffraction limited ablation and enhanced light absorption at the focal spot [29]. Irradiation-induced blebs present a unique opportunity to

utilize a controlled, focused stimulus for the initiation and examination of specific cellular processes. Towards this goal, we report on the capability of laser pulses to initiate GPMV formation and the underlying properties of the blebs. We examine the GPMV pressure gradients, internal viscosity, F-actin distribution, caspase activity, membrane permeability, and phosphatidylserine (PS) externalization of the resulting GPMVs.

2 Materials and methods

Within this manuscript, many fluorophores, cell lines, and rheological techniques were utilized. A brief description is given below and a detailed description is found in the Electronic supplementary material. Additionally, figures labeled with an 'S' are in the Electronic supplementary material.

Cell lines Ten different cell lines were examined to determine the generality of these results, including continuous human epithelial lines (KB, FaDu, A431, MCF-7, MCA-207, Jar, and Jeg-3), primary epithelial lines (UMSCC-22A), rat fibroblasts (Rat2), and mouse red blood cells. MCF-7 cells are unique among this set because they are deficient in caspase-3 activity [30]. MCA-207 cells were transfected with cytosolic green fluorescent protein (GFP). All experiments were performed at 37°C and repeated on a minimum of 12 individually irradiated cells over a variety of cell passages.

Fluorophores Propidium iodide (PI), 10 kD anionic dextran-Alexa Fluor 488, 40 kD anionic dextran-Alexa Fluor 488, Annexin V-Alexa Fluor 488, rhodamine 110-bis(L-aspartic acid amide)$_2$ (R110-AAA$_2$), and phalloidin-Alexa Fluor 488 were obtained from Invitrogen Corp. PI was added to the cell media at various times (spanning 2 h before to 2 h after irradiation) and various concentrations (1–10 μg/mL) with identical staining pattern in all vesicle forming cells. Dextran (25 mg/mL) was added to the cells at least 10 min before irradiation. Annexin V in phosphate-buffered saline (PBS; 10 μL:2 mL) was added to the cells at various times (spanning 40 min before to 40 min after irradiation). R110-AAA$_2$ (60 μM) was added to the cells 45 min before irradiation. Phalloidin-Alexa Fluor 488 (210 nM) was added to the cells at various times (spanning 20 min to 40 min after irradiation) and was occasionally rinsed after irradiation.

Caspase inhibition Two-hour incubation with 22 μM Z-Val-Ala-Asp(OCH_3)-fluoromethylketone (Z-VAD-fmk, Biomol International L.P.) was used to reduce the induction of caspase activity upon cellular stresses [13, 31].

Microscopy setup Epifluorescent micrographs were captured for single-particle tracking (SPT) at 15 frames per second for up to 40 s duration with a DP30 CCD camera on an IX81 inverted microscope with a 100× oil immersion, 1.35 NA UPlanAPO objective (Olympus America, Inc.; Electronic supplementary material, Fig. S5). Fluorescent images were processed with GIF Movie Gear (Gamani Productions), Photoshop CE (Adobe Systems, Inc.), and Matlab (Mathworks, Inc.) to digitally zoom in, adjust contrast and brightness of the entire image, and track the fluorescent beads.

Laser setup A solid-state pump laser (Verdi 532 nm, Coherent, Inc. at 5 W) and a passively mode-locked Ti:sapphire laser (Femtosource Scientific, Femtolasers, Inc.) were used. Laser pulses had a central wavelength of 790 ± 10 nm with a full width at half-maximum of 115

± 10 nm, repetition rate of 90 ± 5 MHz, compressed pulse duration of 9 ± 5 fs, 300 ± 60 mW time average power, and 3 ± 1 nJ/pulse. Laser pulses were transmitted through the 100× oil immersion inverted microscope objective and were expected to be 60 ± 10 fs in duration after transmission through the objective [32]. Laser irradiation of cells occurred for a duration of 0.1 s, which was generally sufficient to induce cavitation within the cytoplasm.

Fluorescent beads Fluorescent beads (Duke Scientific Corp.) were incubated with cells at 3.7 mg/mL for 3 to 5 h before irradiation. The beads were 65 nm diameter polystyrene, carboxylic-acid-coated, and fluorescent at wavelengths similar to fluorescein (absorb at 490 nm, emit at 520 nm). Beads were internalized through natural, endocytotic uptake mechanisms of the cell, as described previously [33].

Diffusion theory and terminology SPT was utilized here to determine the viscosity and structure of GPMVs. The mean-square displacement (MSD) of the particle's position $x(t)$ is proportional to the time step, Δt, such that:

$$\mathrm{MSD}\,(\Delta t) \equiv \left\langle |\mathbf{x}\,(t) - \mathbf{x}\,(t+\Delta t)|^2 \right\rangle_t = 2nD\Delta t \tag{1}$$

where D is the diffusion constant and n is the system dimensionality (e.g., 1D, 2D, or 3D). The viscosity, μ, of the surrounding media can also be calculated from tracking the diffusion of a particle of known radius, r, according to:

$$\mu = \frac{k_\mathrm{B} T}{2\pi n D r}, \tag{2}$$

with Boltzmann's constant k_B, and temperature T. The term "true viscosity" is reserved for the viscosity measured by small particles (≤5 nm diameter) that are affected only by the viscosity of the solvent, while the term "effective viscosity" is used to represent the results from larger particles which are affected both by the solvent and molecular crowding.

3 Results

3.1 Irradiation and vesicle formation

Femtosecond laser pulses were used to stimulate extracellular GPMV formation, or blebbing, on individual living cells. The initial effect of laser irradiation was the creation of short-lived gas-filled micro-bubbles (0.5 to 5 μm diameter) within the cytoplasm of the cell (15 to 30 μm diameter). The micro-bubble formation, or cavitation, occurred within 0.1 s of laser pulse exposure and lasted less than 3 s, similar to micro-bubbles observed previously [34, 35]. Micro-bubble size was controlled with incident laser intensity, focus, and pulse duration; greater incident power resulted in larger and/or numerous micro-bubbles.

With the laser properties used throughout these studies (3 nJ/pulse, 90 MHz, 60-fs duration), a 0.1 s exposure of the cells to the incident laser reliably produced a single micro-bubble at the laser focus. The laser-induced blebs were preferentially formed on, but not limited to the plasma membrane closest to the irradiation focus. Any modifications to the setup that resulted in less light intensity at the focal spot reduced the probability of cavitation. For example, slight misalignment of the laser, reduction of the incident power, or elongation of the pulse duration reduced the probability of inducing cavitation. Incident laser light of the same time-average power, but in a continuous rather than mode-locked state, resulted in no cavitation or morphological changes by the cell. Mode-locked

operation, with high peak intensity and multi-photon processes, was required for significant absorption at the focal spot and micro-bubble formation.

Furthermore, the probability of cavitation varied with the location of laser focus on the cells. The greatest probability of cavitation occurred when focused on the cytoplasm of healthy cells. Focusing on the plasma membrane or nucleus reduced the probability of cavitation. Interestingly, it was particularly difficult to cause cavitation in red blood cells, and any cavitation that did occur was shorter lived (<1 s). The incident laser pulses used in this study did not induce cavitation in water or cell growth media.

The smallest micro-bubbles (<1 μm diameter) did not regularly initiate vesicle formation within 10 min. Large micro-bubbles (>3 μm diameter) resulted in large and numerous GPMVs formed within 30 s of irradiation. Micro-bubble and vesicle formation were observed on all nine different adherent cell lines examined (Fig. 1). Only mouse red blood cells did not form GPMVs upon irradiation. We hypothesize that this difference is due to the substantially different spectrin-based cytoskeletal structure of red blood cells vs. the other cell lines examined [36].

Large variation in GPMV size and number was found in similar irradiation events. GPMV growth rates were fastest when the vesicle first started forming and decreased over time. GPMVs continued to grow throughout the 500 min observation period and never showed retraction (Fig. 2 and Electronic supplementary material, Fig. S1). This observation of decreasing growth rate with time is interesting in light of a previous study in which a constant growth rate of GPMV was observed during cell re-adhesion post-trypsinization [1]. These variations highlight a difference between reversible and irreversible blebbing; variations in the stimulus of GPMV formation (e.g. natural vs. stress-induced) can have a profound effect upon vesicle growth rate, growth duration, and possible retraction.

The morphology of laser-induced GPMVs was compared to the GPMVs induced by other common cell stressors: broad-spectrum UV light, hypotonic solutions, and physical rupture. GPMVs from either the UV light or the physical rupture appeared morphologically identical to the laser-induced vesicles; the vesicles were optically homogeneous, surrounded by a PS containing membrane, and generally spherical. Cells exposed to a hypotonic solution displayed stress and some vesicle formation; however, the vesicle morphologies were considerably different. Cells in a hypotonic environment expanded uniformly and did not tend to make localized, spherical vesicles on the plasma membrane.

3.2 Membrane permeability and GPMV contents

The flow of fluid into GPMVs from the cytoplasm and from the surrounding media was observed via the flow of 10 kDa dextran, 40 kDa dextran, PI, and phalloidin. Before irradiation, dextran did not interact with any particular cellular component, but was slowly taken into the cytoplasm by pinocytosis [37]. Before irradiation, cells incorporated some dextran, but the concentration of dextran in the surrounding media was greater than the concentration in the cytoplasm, as determined by relative fluorescence intensity. Five minutes after irradiation, the concentrations of dextran in the cytoplasm and bleb of the irradiated cell were greater than the surrounding, unirradiated cells, but still less than the surrounding solution (Fig. 3a–d). The surrounding solution was then replaced with fresh PBS to demonstrate the bright fluorescence of the irradiated cell in comparison to the background fluorescence and the unirradiated cells. This indicated that irradiation-induced membrane permeability was sufficient for the flow of 10- and 40-kDa molecules from the

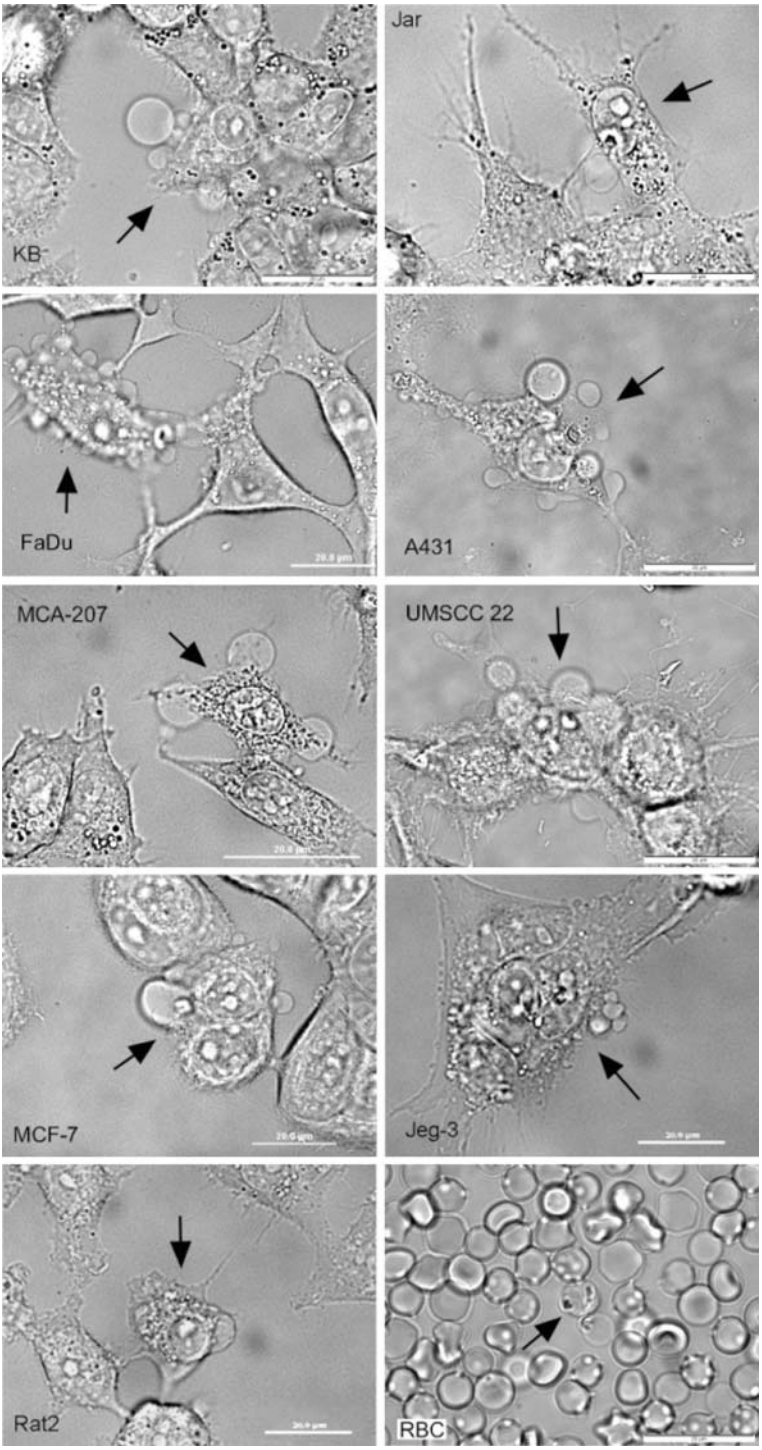
KB-
Jar
FaDu
A431
MCA-207
UMSCC 22
MCF-7
Jeg-3
Rat2
RBC

◀ **Fig. 1** Pulsed-laser irradiation (790 nm, 62 fs, 3 nJ/pulse, 90 MHz) induces micro-bubble formation and GPMV formation in both continuous and primary human cell lines and a rat fibroblast line. Each bright field micrograph shows one irradiated cell (as indicated by the *arrow*) and vesicle formation on the plasma membrane. Micrographs also include control cells within view for direct observation of the effects of irradiation. The varieties of GPMVs shown here are also present in cells within a single cell line. The cellular response to irradiation is not specific to any particular cell type, but rather seems to be a general response to pulsed-laser irradiation by cells. An interesting exception is found for mouse red blood cells (*RBCs*) which, although clearly damaged, do not form vesicles as a result of irradiation, as shown in the *bottom right* image

surrounding solution into the cytoplasm and the bleb and that dextran did not concentrate within the cell.

PI is a small molecule that was used to test membrane integrity because it cannot enter a cell with an intact plasma membrane. When PI enters a cell, it fluoresces brightly, binds to nucleic acids, and accumulates within the cell. PI entered irradiated cells immediately (<30 s) after irradiation and continued to enter cells for up to 2 h after irradiation (Fig. 3e–f). The irradiated cells presumably never recovered their membrane integrity, as expected for necrotic cells.

Flow of material from the cytoplasm to the GPMV was observed in GFP-expressing cells (Fig. 3g–h). The GFP initially was distributed throughout the cytosol, not bound to any particularly cellular protein. Upon blebbing, GFP entered the bleb immediately. This shows that material flows from the cytoplasm to the GPMV. Over time, the intensity of the GFP fluorescence signal from the entire irradiated cell decreased relative to the neighboring control cells. This is consistent with the hypothesis that material escapes from the cytoplasm into the surrounding media upon irradiation (Fig. 3h). GFP was never directly observed in the extracellular media; however, dilution would make the fluorescence undetectable.

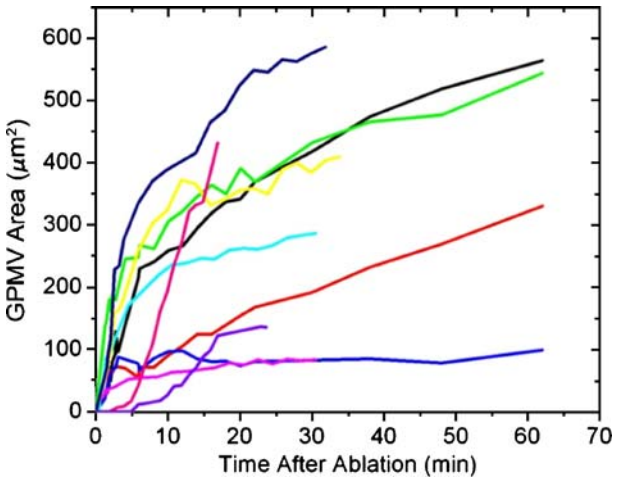

Fig. 2 GPMV growth begins soon after irradiation, usually within the first 30 s. Generally, vesicles' growth rates decrease soon after they were initiated; however, they do not reach a final size within 60 min (for an example over 500 min, see Electronic supplementary material, Fig. S1). The vesicle volume can be estimated by assuming a spherical vesicle, in which case, these results do not change significantly. These data have a 10% uncertainty due to errors in visual vesicle edge determination and variation in microscope focal plane height relative to the largest vesicle cross-sectional area

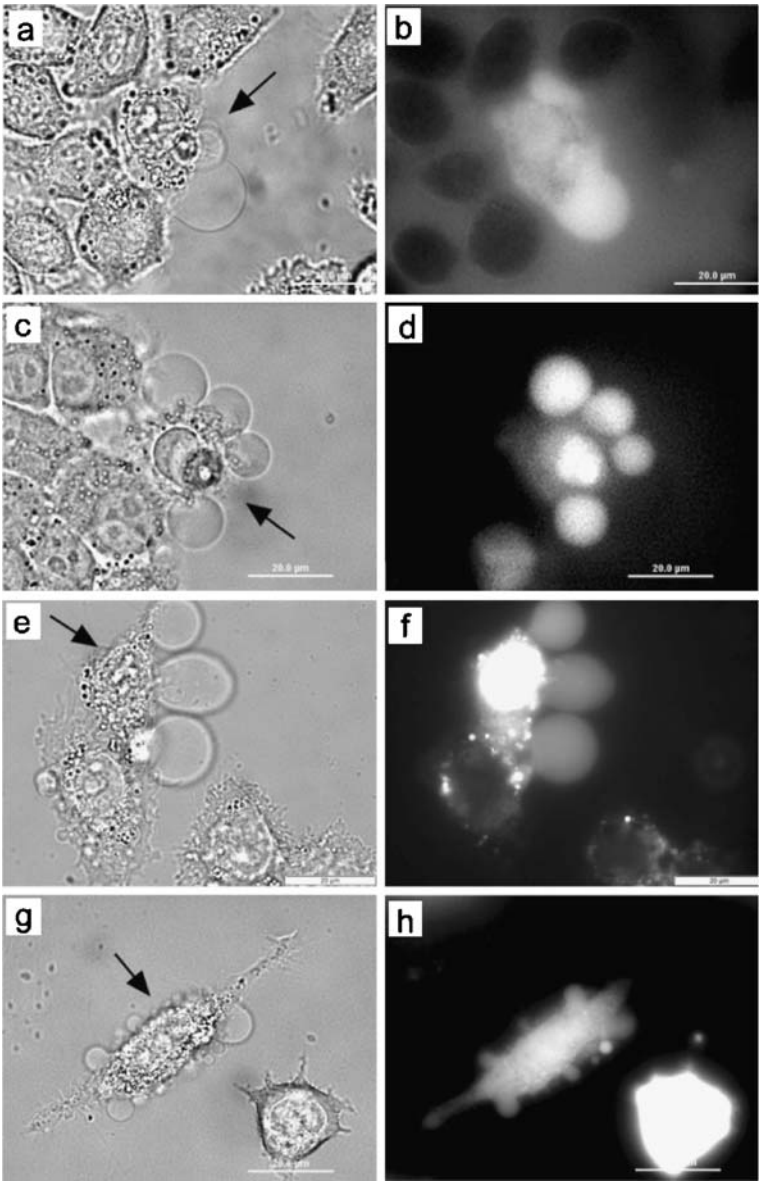

Fig. 3 Material flows from the surrounding media into the irradiated cell, from surrounding media into GPMVs, and from the cytoplasm into the GPMVs of irradiated cells. The irradiated cell in each bright field micrograph is indicated by the *arrow* and is surrounded by control cells. The KB cells at 37°C were surrounded by 40 kDa anionic dextran-AlexaFluor 488 (**a**, **b**), 10 kDa anionic dextran-Alexa Fluor 488 (**c**, **d**), or propidium iodide (**e**, **f**). MCA-207-cytosolic GFP cells (**g**, **h**) were irradiated and emitted fluorescence from both the cytoplasm as well as the GPMVs. The difference in fluorescence intensity from the irradiated and control GFP-expressing cells indicates that cytoplasmic material is also released from the irradiated cell

The F-actin filaments in the cytoplasm and the vesicle were examined with phalloidin-Alexa Fluor 488. Phalloidin bound strongly to F-actin and was observed throughout the cytoplasm and the vesicle after irradiation (Fig. 4). Long filaments of F-actin were observed

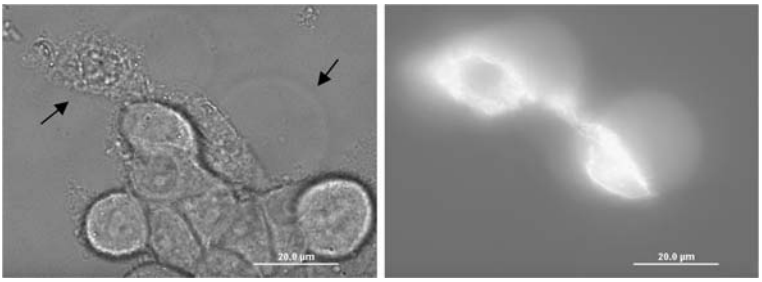

Fig. 4 The GPMVs of irradiated cells incorporate F-actin without any filamentary structure at 37°C. Bright field and fluorescence micrographs of two irradiated KB cells and approximately nine control cells in a PBS solution containing phalloidin-Alexa Fluor 488 are shown. GPMV formation and strong fluorescence were observed for both irradiated cells, as indicated by *arrows*. The phalloidin was presumed to be bound to F-actin and to collect in the cell and GPMVs due to their increased brightness with respect to the surrounding media before the excess phalloidin is rinsed off. The concentration of phalloidin in the cytoplasm is clearly higher than that in the GPMV; however, carefully chosen brightness and contrast settings show both filamentary structure through the cytoplasm and uniform fluorescence throughout the GPMV significantly higher than the background

throughout the cytoplasm; however, no filaments were observed in the GPMVs. This confirms that material flows from the cytoplasm into the bleb. These experiments also show that the bleb contains actin, however not in long filaments.

3.3 Caspase effects

The biochemical effects of laser irradiation were tested through fluorescent studies with (R110-AAA_2). R110-AAA_2 is only fluorescent after cleavage by caspase. The presence of caspases indicates the biochemical cascade associated with apoptosis and eventual cell death. Irradiated cells displayed strong R110-AAA_2 fluorescence and thus caspase activity (Fig. 5).

GPMV activity was also analyzed in MCF-7 cells, which lack caspase-3, to test the contribution of caspase-3 in the cellular response to irradiation. Irradiated MCF-7 cells

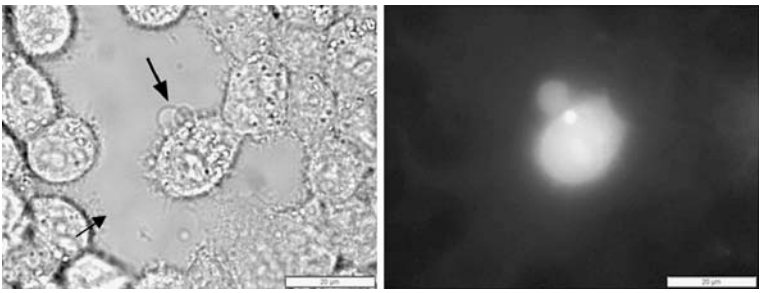

Fig. 5 Irradiation activates the caspase cascade at 37°C. Bright field and fluorescence micrographs of a single irradiated KB cell in the *middle of each panel* (as indicated by the *arrow*) surrounded by many control cells are shown. The surrounding PBS solution contains rhodamine 110 bis(L-aspartic acid amide)$_2$ (*R110-AAA_2*). R110-AAA_2 is capable of entering all cells, but only fluoresces upon cleavage by caspase proteases. Fluorescence is observed in both the cytoplasm and the vesicles of the irradiated cell

displayed similar vesicle formation and R110-AAA_2 fluorescence as all other adherent cells examined. This result indicates that caspase-3 was not essential for vesicle formation or R110-AAA_2 cleavage and that other caspases were activated by irradiation.

Further, Z-VAD-fmk was used to inhibit the presence of all caspases in MCF-7 cells. Cells that were incubated with both Z-VAD-fmk and R110-AAA_2 before irradiation displayed the identical blebbing response as all adherent cells, but displayed no R110-AAA_2 fluorescence. These results show that pulsed-laser initiation of GPMVs does not require the caspase biochemical pathway.

3.4 PS externalization

The molecular composition of the vesicle wall was characterized with Annexin V-Alexa Fluor 488 to assess the presence of PS lipid molecules. Annexin V is commonly used to track PS, and Annexin V cannot enter cells with intact plasma membranes. Within 20 min of irradiation, Annexin V bound to the plasma membrane of the main cell body and GPMV wall (Fig. 6). This indicated that the bleb wall contained phospholipids and suggested that irradiation induced PS externalization to the extracellular plasma membrane leaflet.

Due to the permeability of the membrane induced by irradiation, Annexin V was not assumed to be on the outside of the cell. However, attempts to internalize Annexin V using both electroporation and microinjection showed no intracellular signal from the plasma membrane or organelles. This negative result is consistent with current understanding that intracellular PS was bound to the cytoskeleton and not available for Annexin V binding. Therefore, it is hypothesized that Annexin V was bound to PS on the extracellular side of the plasma membrane and bleb membrane of irradiated cells.

3.5 Intra-vesicle SPT

The viscosity of beads within GPMVs was quantified with SPT of internalized 65 nm fluorescent beads. During incubation of the beads with the cells before irradiation, five to 15 beads were internalized into each cell via natural uptake mechanisms [33]. After irradiation, roughly 5% of the GPMVs incorporated a bead. Bead diffusion was imaged at 15 frames per second and analyzed with a custom software routine to extract the bead location vs. time. From this data, the MSD and the diffusion constant were calculated and obstacles

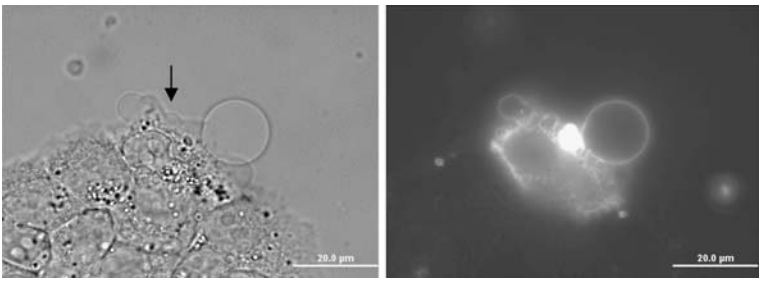

Fig. 6 Irradiated cells externalize PS lipids on all the exposed cell membranes. Bright field and fluorescent micrographs of KB cells surrounded by Annexin V-Alexa Fluor 488 and binding buffer at 37°C are shown. The single irradiated cell (as indicated by the *arrow*) is atop a group of about eight other cells also within view. The control cells show no PS externalization. The irradiation focal spot shows brightest on the fluorescence image

to free diffusion were identified. These results were interpreted as an effective viscosity of the vesicle contents since the bead's motion was affected by the other contents of the bleb. Some bead trajectories revealed obstacles within the vesicle that limited free diffusion (Fig. 7). Identical SPT experiments were attempted on UV-light-induced vesicles. However, such experiments were infeasible because ~0.05% of UV-induced vesicles incorporated a fluorescent bead.

Examination of the bead's free vs. restricted diffusion throughout the vesicle revealed important information about the internal vesicle structure. A bead trajectory with free diffusion throughout the vesicle is shown in Fig. 7a–c. Thirty percent of all beads in blebs interacted with the outer vesicle wall and 40% interacted with some other optically transparent structure within the vesicle (Fig. 7d–f). The MSD vs. Δt for two beads are shown in the Electronic supplementary material, Fig. S2, where the freely diffusing bead yields MSD proportional to Δt and the highly restricted bead displays MSD proportional to $(\Delta t)^{\alpha}$ with $\alpha = 0.65$.

The measured effective viscosities did not display a correlation between magnitude of viscosity and amount of confinement within the vesicle; therefore, these measured viscosity values represent the effective viscosity for a 65 nm bead within the vesicle. Seventy percent of the beads in vesicles were unable to diffuse freely throughout the vesicle. Many of these trajectories were unable to yield useful effective viscosity values due to their rapid obstacle collision rate as compared to the image capture rate. Beads that were free to diffuse at least 300 nm in every dimension were suitable for determining the diffusion constant and the effective viscosity of their surrounding media (Fig. 8). The observed vesicle viscosities

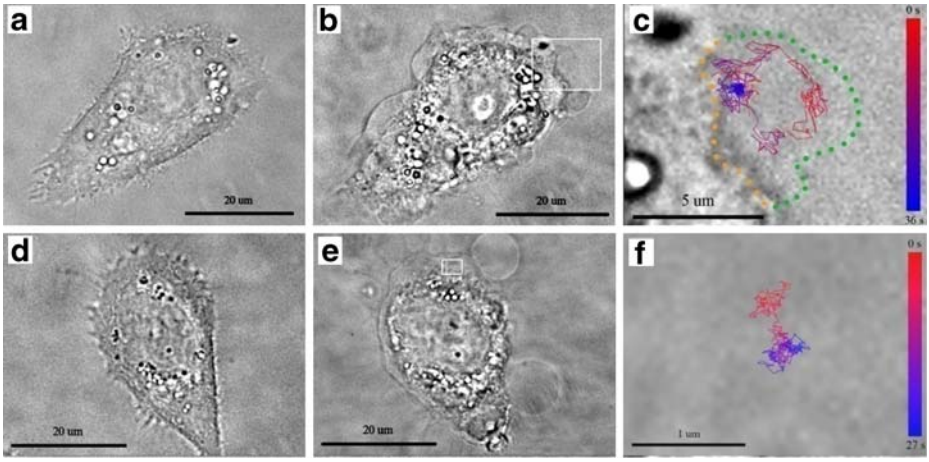

Fig. 7 The GPMVs of irradiated cells incorporate fluorescent beads, which can be tracked. **a**, **d** Before irradiation; **b**, **e** post-irradiation; and **c**, **f** bead trajectory micrographs of KB cells at 37°C are shown. **c**, **f** Magnifications of the *rectangles* in **b**, **e**, respectively. GPMV formation occurs on all non-adherent sections of the plasma membrane, encompasses a large portion of the exterior cell surface, and occasionally shows highly spherical shape. In **c**, the bead moves throughout the vesicle without significant interaction with an interior vesicle structure; the effective viscosity within this vesicle is 220 cP. In **f**, the bead is constrained to a small portion of the vesicle by some optically transparent inner vesicle structure. The collision rate between the bead and the inner vesicle structure in **f** is too high to be determined by our experimental setup. The *color bar* in **c**, **f** represents the time course of the bead's trajectory. In **c**, *green dots* guide the eye around the vesicle and *orange dots* indicate the vesicle–plasma membrane interface

varied from 32 to 434 cP, with a mean of 160 ± 110 cP and 8% random error on all measurements.

The beads used in this study were 65 nm in diameter. Both larger (200, 390, 780 nm diameter) and smaller (40 nm diameter) beads were tested, but did not allow for convenient SPT within the vesicles. All beads were internalized into the cytoplasm during the pre-irradiation incubation. However, the larger beads had a decreased likelihood of entering the GPMV, possibly due to restrictions in the cytoplasm preventing their flow into the GPMV. Smaller beads did not emit enough fluorescence for adequate SPT in this experimental setup. To accommodate these experimental requirements, the 65 nm beads were used exclusively for the data presented throughout this paper.

4 Discussion

4.1 GPMV formation processes

Laser irradiation resulted in a physical stimulus for blebbing. Via inducing micro-bubble formation, multi-photon absorption of the pulsed laser irradiation generated intense pressure and heat within the cytoplasm. Physical stimuli, such as applied hydrostatic pressure gradients on the plasma membrane, previously have been shown sufficient to induce GPMV formation [3, 5–7, 21, 38, 39]. We have identified two likely components to the physical stimuli of irradiation resulting in vesicle formation: cortical actin rupture and osmotic pressure gradients. The rupture component consists of micro-bubble formation causing a large pressure increase within the cytoplasm that breaks the plasma membrane–cytoskeleton interface. Because of cortical actin rupture, the plasma membrane loses its structural support and GPMVs form when the cell's natural pressure gradients are no longer counteracted by the cytoskeleton. The osmotic pressure component may have originated from micro-bubble formation inducing actin depolymerization and significant osmotic pressure increase within the cell. The increased osmotic pressure gradient was relieved by the incorporation of surrounding media into the cytoplasm. However, the influx of fluids into the cytoplasm

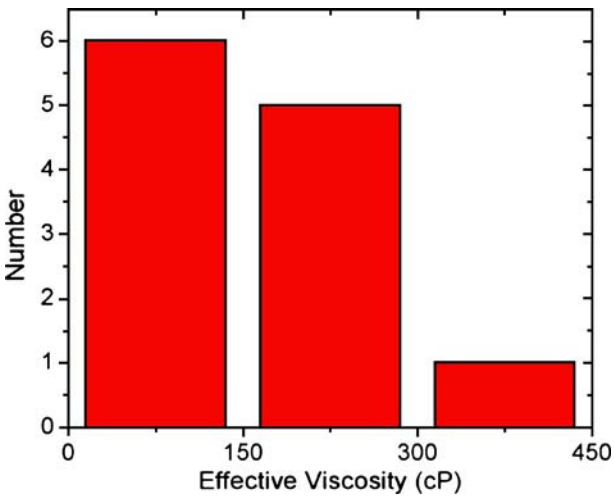

Fig. 8 Histogram of measured effective viscosities in GPMVs. Observed viscosities range from 32 to 434 cP and lower viscosities were more common. The average effective viscosity of the 65 nm beads is 160 ± 110 cP, a wide distribution of observed viscosities. The uncertainty of each viscosity measurement is 8%, as demonstrated in Electronic supplementary material, Fig. S4

resulted in an increase in hydrostatic pressure, which in turn was relieved through blebbing. Since the micro-bubble condensed onto itself within seconds after irradiation, the micro-bubble itself did not result in sustained hydrostatic pressure to promote vesicle growth.

Through analysis of other cellular stressors, rupture was identified as necessary for GPMV formation. By exposing the cells to a hypotonic solution, the cells increased in volume but did not commonly form distinct vesicles. This suggests that only when a physical rupture event is able to cause asymmetry of the cortical actin does the plasma membrane detach from the cytoplasm and form distinct blebs. Thus, an osmotic force alone was not sufficient to induce GPMV formation.

4.2 GPMV morphology and structure

Individual blebs varied in size, shape, and abundance. Some blebs contacted the cell over a relatively small portion of the cell surface and possessed a highly spherical shape. Other blebs made contact with a significant portion (>15%) of the total cell surface and had an irregular, non-spherical shape. These two types of blebs represent the range of blebs observed. Blebs have been similarly categorized by Keller et al. [3] However, Keller et al. distinguished vesicle types by cortical and cytoplasmic actin layers, whereas this research utilized the vesicle shape and area of interaction with the cell surface. All vesicles in which the effective viscosity was measured have been classified by vesicle type, as shown in the Electronic supplementary material, Fig. S3. No significant trend between vesicle type and effective viscosity was observed.

The highly spherical nature of some vesicles suggested that the vesicles were under considerable surface tension and increased hydrostatic pressure as compared to the surrounding media. The hydrostatic pressure that maintained the vesicle's spherical shape and counteracted the membrane surface tension would also have resisted the net flow of material into the vesicle. However, individual concentration gradients may have facilitated the flow of select species against this hydrostatic pressure gradient. To maintain non-spherical shapes, other vesicles appeared to be under less hydrostatic pressure and/or have increased cytoskeletal framework. Annexin V staining indicated that the membranes surrounding all vesicles include PS lipid molecules. Phalloidin staining showed F-actin in all blebs, but none with well-defined filaments in either vesicle type. Thus, these different types of blebs did not clearly differ in surrounding membrane or internal actin.

4.3 Viscosity within GPMVs

The diffusion of small particles within GPMVs revealed fundamental characteristics of the vesicle rheology. The effective viscosity within the bleb was determined to be 160 ± 110 cP. This wide range of observed viscosities demonstrates the wide range of environments within different GPMVs. Beads that were confined to regions less than 300 nm wide within a bleb frequently collided with diffusion barriers and could not be analyzed with a 15-frame per second imaging rate. However, a trend was observed between area of confinement and measured effective viscosity, and all beads gave insight to the inner GPMV structure.

The observed viscosities in cells have been shown to vary greatly with the size of the diffusing probe [40–43]. Here, we observe a range of viscosities of 65 nm diameter beads, presumably due to varying amounts of molecular crowding between blebs. Thus, the observed diffusion of the beads within GPMVs did not represent the true viscosity of the surrounding solvent, but rather a combination of solvent viscosity and collisions with

intra-bleb restrictions to free diffusion. The observed effective viscosity within the GPMV was approximately 50-fold higher than previously determined true viscosity of the cytosol [42, 44].

The diffusion of 65 nm diameter beads was measured in the cytosol before irradiation. However, all beads within the cytoplasm appeared to be highly confined in each dimension, never moving >100 nm between image frames. This experimental setup was never capable of measuring the viscosity of the cytosol due to the high collision rate of the beads with optically transparent, cytoplasmic structure. This result demonstrates that GPMVs contained significantly less obstructions to diffusion than the cytoplasm.

As purchased, beads were expected to be homogeneous. Within the cell, the carboxylic-acid-coated beads may have changed size and surface properties. This is a common problem with the incorporation of any well-characterized material into a biological system and has been previously referred to as a "corona," which adds to the uncertainty of these results [45]. However, such protein and membrane layers typically do not exceed $\sim$10 nm thickness, which is considerably smaller than the expected particle radius change needed to otherwise explain the observed tenfold variation in diffusion rates.

4.4 GPMV actin contents

Phalloidin was observed homogeneously throughout the GPMV without any filamentary structure (Fig. 4). Phalloidin was an effective indicator of F-actin, reduced the rate of actin filament depolymerization, and prevented conversion of F-actin to G-actin [46]. It is not clear how the F-actin became distributed throughout the vesicle, since non-filamentary actin is expected to be in the G form and unavailable for phalloidin binding. We hypothesize the following progression: (1) the phalloidin enters the cytoplasm through the permeable plasma membrane of the irradiated cell and binds to F-actin filaments, (2) the osmotic and hydrostatic pressure imbalances that fuel the GPMV growth induce F-actin disassembly, and (3) the short segments of F-actin bound to phalloidin are flushed into the growing vesicle along with other cytoplasmic particles. This hypothesis accommodates both the common understanding of phalloidin activity and our observation of both concentrated phalloidin and non-filamentary actin within the vesicle.

At first glance, the fluorescent images presented in Fig. 4 do not clearly show that the fluorescence signal within the vesicle was directly due to phalloidin vs. a reflection/refraction of fluorescence from the GPMV. However, in Fig. 4, the control cells, in close proximity to the irradiated cells within the same micrograph, display none of this reflection effect. These results demonstrate the power of the pulsed-laser irradiation method utilizing control cells in very close proximity to stressed cells. Furthermore, transmission electron micrographs of irreversible blebs caused by oxidative stress support the presence of low-density cytoplasmic material throughout the vesicle [47].

5 Conclusions

Pulsed-laser irradiation was used for the generation of vesicles on individual cells in vitro. These vesicles were analyzed with fluorescence and bright field microscopy for quantification of GPMV properties and the overall cellular response to irradiation. The

blebs resulting from laser irradiation were similar to membrane vesicles occasionally called blisters, since they were created from injury, had no F-actin structure, and were irreversible. The constancy of this observation among a variety of cell lines indicates that this is a common cellular response to femtosecond laser irradiation in living animal cells. The vesicles are described in terms of the source of the material that fills them, the biochemical and physical mechanisms of their formation, and their structural properties. The use of pulsed-lasers to initiate blebbing demonstrates a mechanism of inducing membrane vesicle formation, which could be used in a variety of GPMV studies. This characterization of the blebbing process and the physiochemical properties of the resulting GPMVs provides the foundation for such studies.

Acknowledgments Partial support for this project was provided by the Michigan Nanotechnology Institute for Medicine and Biological Sciences, the National Institute of Biomedical Imaging and Bioengineering (R01-EB005028), and by the NSF Frontiers in Physics FOCUS Center under grant PHY-0114336. C.V.K. received fellowship support from the NIH Michigan Molecular Biophysics Training Program (T32 GM008270-20), the Applied Physics program, and the Graham Environmental Sustainability Institute. The authors thank Meghan Liroff, Tom Dunham, Pascale Leroueil, Kevin McDonough, Alina Kotlya, and Kathryn Kelly.

References

1. Cunningham, C.C.: Actin polymerization and intracellular solvent flow in cell-surface blebbing. J. Cell Biol. **129**, 1589–1599 (1995). doi:10.1083/jcb.129.6.1589
2. Hagmann, J., Burger, M.M., Dagan, D.: Regulation of plasma membrane blebbing by the cytoskeleton. J. Cell. Biochem. **73**, 488–499 (1999). doi:10.1002/(SICI)1097-4644(19990615)73:4<488::AID-JCB7>3.0.CO;2-P
3. Keller, H., Rentsch, P., Hagmann, J.: Differences in cortical actin structure and dynamics document that different types of blebs are formed by distinct mechanisms. Exp. Cell Res. **277**, 161–172 (2002). doi:10.1006/excr.2002.5552
4. Paluch, E., van der Gucht, J., Sykes, C.: Cracking up: symmetry breaking in cellular systems. J. Cell Biol. **175**, 687–692 (2006). doi:10.1083/jcb.200607159
5. Charras, G.T., Yarrow, J.C., Horton, M.A., Mahadevan, L., Mitchison, T.J.: Non-equilibration of hydrostatic pressure in blebbing cells. Nature **435**, 365–369 (2005). doi:10.1038/nature03550
6. Rentsch, P.S., Keller, H.: Suction pressure can induce uncoupling of the plasma membrane from cortical actin. Eur. J. Cell Biol. **79**, 975–981 (2000). doi:10.1078/0171-9335-00124
7. Sheetz, M.P., Sable, J.E., Dobereiner, H.G.: Continuous membrane–cytoskeleton adhesion requires continuous accommodation to lipid and cytoskeleton dynamics. Annu. Rev. Biophys. Biomol. Struct. **35**, 417–434 (2006). doi:10.1146/annurev.biophys.35.040405.102017
8. Boulbitch, A., Simson, R., Simson, D.A., Merkel, R., Hackl, W., Barmann, M., Sackmann, E.: Shape instability of a biomembrane driven by a local softening of the underlying actin cortex. Phys. Rev. E **62**, 3974–3985 (2000). doi:10.1103/PhysRevE.62.3974
9. Charras, G.T.: A short history of blebbing. Paper presented at the 6th Abercrombie symposium on cell motility, Oxford, England (2007)
10. Rafelski, S.M., Theriot, J.A.: Crawling toward a unified model of cell motility: spatial and temporal regulation of actin dynamics. Annu. Rev. Biochem. **73**, 209–239 (2004). doi:10.1146/annurev.biochem.73.011303.073844
11. Charras, G., Paluch, E.: Blebs lead the way: how to migrate without lamellipodia. Nat. Rev. Mol. Cell Biol. **9**, 730–736 (2008). doi:10.1038/nrm2453
12. Jungbluth, A., Vonarnim, V., Biegelmann, E., Humbel, B., Schweiger, A., Gerisch, G.: Strong increase in the tyrosine phosphorylation of actin upon inhibition of oxidative-phosphorylation—correlation with reversible rearrangements in the actin skeleton of dictyostelium cells. J. Cell Sci. **107**, 117–125 (1994)
13. Mills, J.C., Stone, N.L., Erhardt, J., Pittman, R.N.: Apoptotic membrane blebbing is regulated by myosin light chain phosphorylation. J. Cell Biol. **140**, 627–636 (1998). doi:10.1083/jcb.140.3.627

14. Charras, G.T., Hu, C.K., Coughlin, M., Mitchison, T.J.: Reassembly of contractile actin cortex in cell blebs. J. Cell Biol. **175**, 477–490 (2006). doi:10.1083/jcb.200602085
15. Ilegems, E., Pick, H.M., Deluz, C., Kellenberger, S., Vogel, H.: Noninvasive imaging of 5-HT3 receptor trafficking in live cells—from biosynthesis to endocytosis. J. Biol. Chem. **279**, 53346–53352 (2004). doi:10.1074/jbc.M407467200
16. Sengupta, P., Baird, B., Holowka, D.: Lipid rafts, fluid/fluid phase separation, and their relevance to plasma membrane structure and function. Semin. Cell Dev. Biol. **18**, 583–590 (2007). doi:10.1016/j.semcdb.2007.07.010
17. Barros, L.F., Kanaseki, T., Sabirov, R., Morishima, S., Castro, J., Bittner, C.X., Maeno, E., Ando-Akatsuka, Y., Okada, Y.: Apoptotic and necrotic blebs in epithelial cells display similar neck diameters but different kinase dependency. Cell Death Differ. **10**, 687–697 (2003). doi:10.1038/sj.cdd.4401236
18. Gores, G.J., Herman, B., Lemasters, J.J.: Plasma-membrane bleb formation and rupture—a common feature of hepatocellular injury. Hepatology **11**, 690–698 (1990). doi:10.1002/hep.1840110425
19. Huot, J., Houle, F., Rousseau, S., Deschesnes, R.G., Shah, G.M., Landry, J.: SAPK2/p38-dependent F-actin reorganization regulates early membrane blebbing during stress-induced apoptosis. J. Cell Biol. **143**, 1361–1373 (1998). doi:10.1083/jcb.143.5.1361
20. Sebbagh, M., Renvoize, C., Hamelin, J., Riche, N., Bertoglio, J., Breard, J.: Caspase-3-mediated cleavage of ROCK I induces MLC phosphorylation and apoptotic membrane blebbing. Nat. Cell Biol. **3**, 346–352 (2001). doi:10.1038/35070019
21. Yanai, M., Kenyon, C.M., Butler, J.P., Macklem, P.T., Kelly, S.M.: Intracellular pressure is a motive force for cell motion in Amoeba proteus. Cell Motil. Cytoskelet. **33**, 22–29 (1996). doi:10.1002/(SICI)1097-0169(1996)33:1<22::AID-CM3>3.0.CO;2-K
22. Malorni, W., Straface, E., Donelli, G., Giacomoni, P.U.: UV-induced cytoskeletal damage, surface blebbing and apoptosis are hindered by alpha-tocopherol in cultured human keratinocytes. Eur. J. Dermatol. **6**, 414–420 (1996)
23. Veatch, S.L., Cicuta, P., Sengupta, P., Honerkamp-Smith, A., Holowka, D., Baird, B.: Critical fluctuations in plasma membrane vesicles. ACS Chem. Biol. **3**, 287–293 (2008). doi:10.1021/cb800012x
24. Baumgart, T., Hammond, A.T., Sengupta, P., Hess, S.T., Holowka, D.A., Baird, B.A., Webb, W.W.: Large-scale fluid/fluid phase separation of proteins and lipids in giant plasma membrane vesicles. Proc. Natl. Acad. Sci. U. S. A. **104**, 3165–3170 (2007). doi:10.1073/pnas.0611357104
25. Holowka, D., Baird, B.: Structural studies on the membrane-bound immunoglobulin E-receptor complex. 1. Characterization of large plasma-membrane vesicles from rat basophilic leukemia-cells and insertion of amphipathic fluorescent-probes. Biochemistry **22**, 3466–3474 (1983). doi:10.1021/bi00283a025
26. Tank, D.W., Wu, E.S., Webb, W.W.: Enhanced molecular diffusibility in muscle membrane blebs—release of lateral constraints. J. Cell Biol. **92**, 207–212 (1982). doi:10.1083/jcb.92.1.207
27. Baumann, N.A., Vidugiriene, J., Machamer, C.E., Menon, A.K.: Cell surface display and intracellular trafficking of free glycosylphosphatidylinositols in mammalian cells. J. Biol. Chem. **275**, 7378–7389 (2000). doi:10.1074/jbc.275.10.7378
28. Bauer, B., Davidson, M., Orwar, O.: Proteomic analysis of plasma membrane vesicles. Angew. Chem., Int. Ed. **48**, 1656–1659 (2009). doi:10.1002/anie.200803898
29. Vogel, A., Noack, J., Huttman, G., Paltauf, G.: Mechanisms of femtosecond laser nanosurgery of cells and tissues. Appl. Phys. B **81**, 1015–1047 (2005). doi:10.1007/s00340-005-2036-6
30. Janicke, R.U., Sprengart, M.L., Wati, M.R., Porter, A.G.: Caspase-3 is required for DNA fragmentation and morphological changes associated with apoptosis. J. Biol. Chem. **273**, 9357–9360 (1998). doi:10.1074/jbc.273.16.9357
31. Janicke, R.U., Ng, P., Sprengart, M.L., Porter, A.G.: Caspase-3 is required for alpha-fodrin cleavage but dispensable for cleavage of other death substrates in apoptosis. J. Biol. Chem. **273**, 15540–15545 (1998). doi:10.1074/jbc.273.25.15540
32. Tadepalli, N.R., Alexander, D., Doerr, D., Li, J., Zhang, H.: Femtosecond pulse stretching in microscope objectives used for micro/nanomachining. J. Laser Appl. **17**, 270–272 (2005). doi:10.2351/1.2080287
33. Reece, J.C., Vardaxis, N.J., Marshall, J.A., Crowe, S.M., Cameron, P.U.: Uptake of HIV and latex particles by fresh and cultured dendritic cells and monocytes. Immunol. Cell Biol. **79**, 255–263 (2001). doi:10.1046/j.1440-1711.2001.01011.x
34. Zohdy, M.J., Tse, C., Ye, J.Y., O'Donnell, M.: Optical and acoustic detection of laser-generated microbubbles in single cells. IEEE Trans. Ultrason. Ferroelectr. Freq. Control **53**, 117–125 (2006). doi:10.1109/TUFFC.2006.1588397
35. Vogel, A., Linz, N., Freidank, S., Paltauf, G.: Femtosecond-laser-induced nanocavitation in water: implications for optical breakdown threshold and cell surgery. Phys. Rev. Lett. **100**, 4 (2008)
36. Alberts, B., Johnson, A., Lewis, J., Raff, M., Roberts, K., Walter, P.: Molecular Biology of the Cell, 4th edn. Garland, New York, NY (2002)

37. Vogel, G., Thilo, L., Schwarz, H., Steinhart, R.: Mechanism of phagocytosis in dictyostelium-discoideum—phagocytosis is mediated by different recognition sites as disclosed by mutants with altered phagocytotic properties. J. Cell Biol. **86**, 456–465 (1980). doi:10.1083/jcb.86.2.456
38. Dai, J.W., Ting-Beall, H.P., Hochmuth, R.M., Sheetz, M.P., Titus, M.A.: Myosin I contributes to the generation of resting cortical tension. Biophys. J. **77**, 1168–1176 (1999). doi:10.1016/S0006-3495(99)76968-7
39. Paluch, E., Piel, M., Prost, J., Bornens, M., Sykes, C.: Cortical actomyosin breakage triggers shape oscillations in cells and cell fragments. Biophys. J. **89**, 724–733 (2005). doi:10.1529/biophysj.105.060590
40. Banks, D.S., Fradin, C.: Anomalous diffusion of proteins due to molecular crowding. Biophys. J. **89**, 2960–2971 (2005). doi:10.1529/biophysj.104.051078
41. Guigas, G., Kalla, C., Weiss, M.: Probing the nanoscale viscoelasticity of intracellular fluids in living cells. Biophys. J. **93**, 316–323 (2007). doi:10.1529/biophysj.106.099267
42. Luby-Phelps, K., Taylor, D.L., Lanni, F.: Probing the structure of cytoplasm. J. Cell Biol. **102**, 2015–2022 (1986). doi:10.1083/jcb.102.6.2015
43. Weiss, M., Elsner, M., Kartberg, F., Nilsson, T.: Anomalous subdiffusion is a measure for cytoplasmic crowding in living cells. Biophys. J. **87**, 3518–3524 (2004). doi:10.1529/biophysj.104.044263
44. Mastro, A.M., Keith, A.D.: Diffusion in the aqueous compartment. J. Cell Biol. **99**, S180–S187 (1984). doi:10.1083/jcb.99.1.180s
45. Lynch, I., Dawson, K.A., Linse, S.: Detecting cryptic epitopes created by nanoparticles. Sci. STKE **327**, pe14 (2006). doi:10.1126/stke.3272006pe14
46. Faulstich, H., Zobeley, S., Heintz, D., Drewes, G.: Probing the phalloidin binding-site of actin. FEBS Lett. **318**, 218–222 (1993). doi:10.1016/0014-5793(93)80515-V
47. Miyoshi, H., Umeshita, K., Sakon, M., Imajoh-Ohmi, S., Fujitani, K., Gotoh, M., Oiki, E., Kambayashi, J., Monden, M.: Calpain activation in plasma membrane bleb formation during tert-butyl hydroperoxide-induced rat hepatocyte injury. Gastroenterology **110**, 1897–1904 (1996). doi:10.1053/gast.1996.v110.pm8964416